THE JOURNAL OF PHYSICAL CHEMISTRY B

Article

pubs.acs.org/JPCB

Photophysics and Photochemistry of a DNA–Protein Cross-Linking Model: A Synergistic Approach Combining Experiments and Theory

Marco Micciarelli,[†,‡] Mohammadhassan Valadan,[†] Bartolomeo Della Ventura,[‡] Giovanni Di Fabio,[§] Lorenzo De Napoli,[§] Sara Bonella,[‡] Ursula Röthlisberger,[∥] Ivano Tavernelli,*[,∥] Carlo Altucci,[†] and Raffaele Velotta*[,†]

[†]Department of Physics, University of Naples Federico II, Via Cintia, 26, 80126 Napoli, Italy

[‡]Department of Physics, University of Rome La Sapienza, P.le Aldo Moro 5, 00185 Roma, Italy

[§]Department of Chemical Sciences, University of Naples Federico II, Via Cintia, 26, 80126 Napoli, Italy

[∥]Laboratory of Computational Chemistry and Biochemistry, Ecole Polytechnique Fédérale de Lausanne, CH-1015 Lausanne, Switzerland

Supporting Information

ABSTRACT: The photophysical and photochemical properties of 5-benzyluracil and 5,6-benzyluracil, the latter produced by photocyclization of the former through irradiation with femtosecond UV laser pulses, are investigated both experimentally and theoretically. The absorption spectra of the two molecules are compared, and the principal electronic transitions involved are discussed, with particular emphasis on the perturbation induced on the two chromophore species (uracil and benzene) by their proximity. The photoproduct formation for different irradiation times was verified with high-performance liquid chromatography and nuclear magnetic resonance measurements. The steady-state fluorescence demonstrates that the fluorescence is a distinctive physical observable for detection and selective identification of 5- and 5,6-benzyluracil. The principal electronic decay paths of the two molecules, obtained through TDDFT calculations, explain the features observed in the emission spectra and the photoreactivity of 5-benzyluracil. The order of magnitude of the lifetime of the excited states is derived with steady-state fluorescence anisotropy measurements and rationalized with the help of the computational findings. Finally, the spectroscopic data collected are used to derive the photocyclization and fluorescence quantum yields. In obtaining a global picture of the photophysical and photochemical properties of the two molecules, our findings demonstrates that the use of 5-benzyluracil as a model system to study the proximity relations of a DNA base with a close-lying aromatic amino acid is valid at a local level since the main characteristics of the decay processes from the excited states of the uracil/thymine molecules remain almost unchanged in 5-benzyluracil, the main perturbation arising from the presence of the close-lying aromatic group.

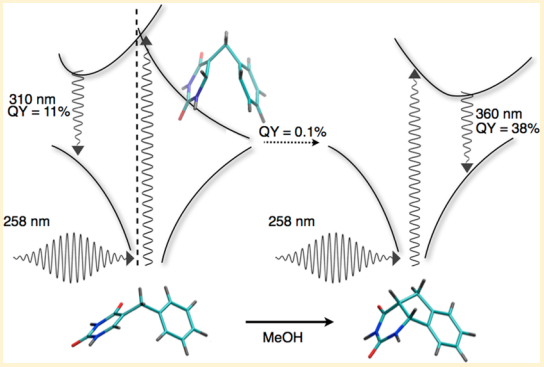

INTRODUCTION

The photophysics of DNA bases has been attracting considerable attention for the inherent interest to study the basic mechanisms that lead to the protection of the DNA strands.[1] In fact, these molecules can be considered as almost perfect machineries in preventing photodamage. In contrast to the long lifetimes of other possible analogous bases not found in DNA and RNA,[2−4] they relax on the electronic ground state by means of both radiative and nonradiative processes in an ultrafast timescale. As a result, their photochemical reactivity is strongly inhibited and the energy accumulated in DNA and RNA by the radiation gets immediately dissipated, suggesting that their actual chemical form may be the fruit of an evolutionary process in the early biotic ages.

At the molecular level the most important photoproducts in the case of low-intensity irradiation of DNA at 254 nm are the cyclobutane-type pyrimidine dimers[5] whose formation has been studied theoretically[6−8] as well as experimentally,[9] even with its dynamics temporally resolved.[10] UV absorption by DNA can also be exploited as a tool to induce DNA–protein cross-link[11−14] in view of the key role this phenomenon plays in biochemical investigations.[15]For instance, the adoption of UV light irradiation in living cells has the unique property of inducing a zero-length cross-linking between DNA and the interacting proteins, namely the establishment of a covalent bond between nucleic acids and the proteins at their contact.[11]

The analysis of the molecular mechanisms underlying UV-induced DNA–protein cross-link (UV-CL in the following) is a formidable task with a microscopic description being far from complete.[13] In an effort to improve the comprehension of such

Received: November 22, 2013
Revised: April 15, 2014
Published: April 17, 2014

dx.doi.org/10.1021/jp4115018 | J. Phys. Chem. B 2014, 118, 4983−4992

a fundamental process, Sun et al. investigated experimentally the cross-linking of tyrosine, phenylalanine, and tryptophan to the pyrimidine bases relying on a simple model-building strategy:[16] they attached the pyrimidine base to the tyrosine, phenylalanine, and tryptophan side chains, using a short and chemically inert linker to mimic the proximity and orientation in DNA−protein complexes. The quantum yield (QY) for UV-CL of such simple models was more than 1 order of magnitude lower than the QY of thymine dimer formation; moreover, no significant two photon contribution was evidenced.[16] While such a simple model is surely distant from the complexity of an actual DNA−protein cross-link "in vivo", it can nevertheless provide useful insights into the molecular mechanism underlying the formation of a covalent bond between DNA bases and protein amino acids. In particular, the UV-induced photocyclization of 5-benzyluracil (5BU) leading to 5,6-benzyluracil (5,6BU) may well-describe possible structures related to the cross-linking of phenylalanine to DNA.[16] Moreover, the 5BU photoreaction, involving a cyclization, can also be contextualized in the study of the dynamics of the ring closure,[17−19]which is widely investigated in the perspective of realizing effective molecular switches.[20]

The goal of this work is to characterize, combining steady-state spectroscopy and electronic structure calculations, the photophysical and photochemical properties of 5-benzyluracil (5BU) in the methanol (MeOH) solution. Experimentally, we have characterized absorption and fluorescence (including its anisotropy) of 5BU and 5,6BU, the latter produced by UV femtosecond pulses photoabsorption, measuring the fluorescence QY as well as the QY of 5,6BU production. To gain further insight on the photophysical and photochemical properties of the two molecules by identifying the electronic states involved in the absorption and emission spectra and the relevant microscopic conformations of reactant and product, we have also studied them using time dependent density functional theory (TDDFT) including solvent effects with a self-consistent reaction field (SCRF) model. The use of TDDFT for the description of the excited state properties of these molecules requires some care:[21,22] while the intrachromophore electronic transitions of the single moieties of 5BU (benzene and uracil/thymine) are well-described by TDDFT,[23] the choice of the exchange correlation (xc) functional can strongly affect the results for the description of the intermonomer charge-transfer (CT) transitions;[24−26] thus, we have explored the performances of different functionals to ensure the reliability of our calculations.

The paper is organized as follows: after Materials and Methods, which includes the details of the experiments as well as of the theoretical calculations, in Results we describe the photophysical and photochemical properties of 5BU and 5,6BU. In particular, we characterize the formation of the photoproduct via absorption and fluorescence measurements. The principal electronic decay paths of the two molecules are also computationally studied to describe and explain the photoreactivity of the 5BU and the features observed in the UV absorption and emission spectra. Conclusions are devoted to summarize the results obtained, and a global picture of the studied processes is provided.

MATERIALS AND METHODS

Chemicals and Spectroscopy Measurements. 5BU powder (purchased from ALCHEMY Fine Chemicals & Research, Italy) was dissolved in methanol 99.8% HPLC grade. The absorbance spectra were acquired with a UV−Vis spectrophotometer device using a quartz cuvette with a path length of 1 cm. The spectra were acquired in the range of 210−380 nm at several concentrations, both for 5BU and 5,6BU, verifying the linearity of the response. The fluorescence emission spectra were measured with a LS55 PerkinElmer spectrofluorometer. The excitation wavelength was 265 nm, and the fluorescence was collected in the range of 290−380 nm. The path length of the fluorescence photons in the cuvette was approximately 1 mm. The same device, with automatic polarizers both in excitation and emission, was used to carry out anisotropy measurements. The measurements were corrected for the grating efficiency factor. 5,6BU was obtained by UV photoirradiation of 5BU by a femtosecond laser system (Light Conversion, Lithuania). This device operates at 258 nm (fourth harmonic of 1032 nm, fundamental wavelength of the IR source PHAROS), 200 fs pulse duration, and a 2 kHz repetition rate, thereby delivering 0.2 W of average power. The sample was constantly stirred with a magnetic bar to have a homogeneous solution while irradiating. For the spectral measurements of the 5,6BU, samples obtained after 1 min exposition to the laser UV laser pulses were used, since we verified that these samples contained only 5,6BU.

HPLC and NMR Measurements. The characterization of the final product after UV laser pulse irradiation of the 5BU was essential to verify the occurrence of the photocyclization process and the consequent complete transformation of 5BU into 5,6BU in the appropriate conditions of irradiations. To this end, we carried out high-performance liquid chromatography (HPLC) and nuclear magnetic resonance (NMR) spectroscopy of the pure and irradiated 5BU. HPLC-grade solvents (Carlo Erba Reagents) were used as received in a Shimadzu LC-8A PLC system equipped with a Shimadzu SCL-10A VP System control and Shimadzu SPD-10A VP UV−Vis detector. ^{1}H NMR was carried out immediately after photoirradiation, and the spectra were recorded in CD_3OH with a Bruker WM 400 spectrometer. For ElectroSpray Ionization Mass Spectrometry (ESI-MS) analysis, a Waters Micromass ZQ instrument, equipped with an electrospray source, was used in the positive mode.

5BU was dissolved in MeOH at a concentration of 0.35 μM. One milliliters of solutions were photoirradiated at 258 nm for 0, 20, and 60 s in a 1 cm long cuvette at room temperature. Immediately after photoirradiation, the samples were dried with a nitrogen flow and redissolved in 50 μL of H_2O/CH_3OH (95/5, v:v) and then injected onto a RP-18 column (Phenomenex LUNA, 5 μm particle size, 10.0 mm × 250 mm i.d.) eluted with a linear gradient from 5 to 95% B in 20 min (A = H_2O, B = CH_3CN; detection at λ = 265 nm; flow rate 1.5 mL/min). The data reveal that photoirradiation of 5BU generates a single product at a retention time of 22.5 min, when 5BU was irradiated for 1 min. The structure analysis by ^{1}H NMR and ESI-MS experiments proved that this compound is the 5,6BU in agreement with the results reported by Sun et al.[16]In particular, we observed the disappearance of the signal of H-6 (7.05 ppm) of uracil portion and subsequent appearance of new H-6 proton signal in upfield (4.95 ppm).

Theoretical Calculations. All calculations were performed applying DFT and TDDFT methods and using Gaussian09.[27] To validate the results obtained, we have systematically tested different xc functionals: the PBE functional[28] in the GGA class of functionals, the M06[29] in the meta-hybrid class of functionals, and the M062X and CAM-B3LYP which are

dx.doi.org/10.1021/jp4115018 | J. Phys. Chem. B 2014, 118, 4983−4992

known to perform well for charge-transfer excitations.[29,30] In all cases, the Dunnings cc-pVDZ correlation consistent basis set[31] was used; tests performed increasing the size of the basis set implied a significant increase of computer time for the calculations without an improvement in the accuracy of the results. For numerical integrations a pruned grid has been used, with 75 radial shells and 302 angular points per shell. As convergence criteria, we used a convergence threshold in energy (1.00×10^{-6} au) and in the root mean square (RMS) of the density matrix of (1.00×10^{-8}).

The solvent was represented implicitly and the solvation effects were taken into account by means of a self-consistent reaction-field (SCRF) model in its integral equation formalism (IEFPCM) variant.[32] In accordance with this model, the solute lies in a cavity created in a dielectric continuum, which represents the solvent. The continuum solvent, characterized by its relative static dielectric permittivity ε_r, is polarized by the solute and hence creates an electric field inside the cavity which is self-consistently computed and added to the molecular electronic Hamiltonian. In our calculations, we have used ε_r = 32.613 to model the MeOH solvation effects.[33]

Full geometry optimizations of the reactant and product in their singlet ground state were performed using all the xc functionals mentioned above. For each ground state optimized geometry, linear response TDDFT (LR-TDDFT) calculations were performed to determine the excited state energies using the corresponding xc-functional. To cover the experimental energy range, the first 10 vertical excitations were computed. The absorption spectrum was modeled with Lorentian functions envelopes: the Lorentian peaks are centered at the excitation energies, their intensities proportional to the oscillator strengths, and the half widths empirically set so as to reproduce the experimental broadening and allow a better comparison with the experimental data.

By comparing the computed absorption spectra with the experimental ones, we found that the best agreement is achieved using the M06 functional. To investigate this somewhat surprising result (CAM-B3LYP is usually recommended when CT transitions are involved, as in our case) we computed the Λ parameter for orbital overlap. This quantity is often used as a diagnostic tool to assess the performances of different functionals.[34] Results are reported in Table S3 in the Supporting Information. They show that for the first two transitions, on which we focus here, all the functionals give Λ values in the range 0.45−0.65. According to the analysis performed by Peach et al.,[34] this is a situation in which CAM-B3LYP can overestimate excitation energies due to an overcorrection of the long-range behavior of the xc functional. In the following, we report and discuss the results obtained using the M06 functional.

Full geometry optimizations of the nuclear positions were performed also on the excited states using the M06 functional (and, for 5BU, also CAM-B3LYP, see the Supporting Information for an explanation of this choice) for the characterization of the electronic decay channels.

RESULTS AND DISCUSSION

Molecular Geometries in the Ground State. In Figure 1, the DFT/M06 ground state structures of the 5BU and 5,6BU in MeOH are reported. In the case of 5BU, the structure shows appreciable differences from the more symmetric geometry obtained in the gas phase (see Figure S1 in the Supporting Information).

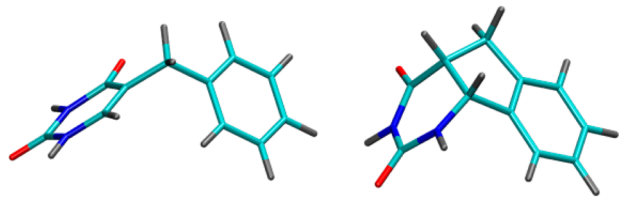

Figure 1. Stick representation of the solvated ground state molecular geometries of 5BU (left) and 5,6BU (right). Carbon atoms are colored in cyan, oxygen in red, nitrogen in blue, and hydrogen in gray.

This distortion is due to a solvent-induced internal rotation around the hinge connecting the two chromophore moieties. Analogous geometrical distortions in the ground state 5BU structure have been observed also using the other xc functionals. The energy difference associated with the alternative structures is less than a k_BT at room temperature (see the Supporting Information for more details).

Photophysical Properties in the Franck−Condon Region. The UV electronic absorption spectra of 5BU and 5,6BU in MeOH were experimentally recorded and computed with LR-TDDFT to characterize the principal electronic transitions.

The experimental and computed absorption profiles of the molecules are reported in Figure 2 (respectively with dashed red line and continuous black line). The data reflect the dramatic electronic structure changes that occur after cyclization. Although the calculated bands show a systematic blue shift, the overall agreement between theory and experiments is sufficient to allow an unequivocal assignment of the transitions.

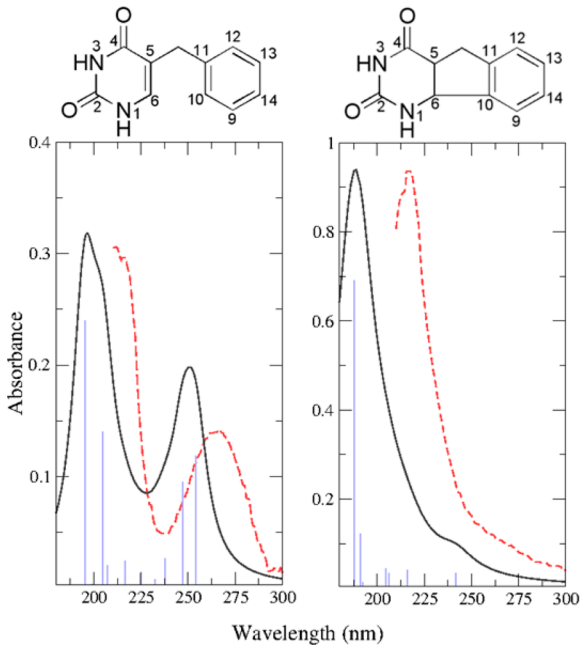

Figure 2. Absorption spectra of 5BU (left) and 5,6BU (right). Experimental spectra (red dashed lines) are shown together with LR-TDDFT/M06 convoluted spectra (continuous black lines). The vertical excitation energies (resonances) are represented by blue bars with a height corresponding to the oscillator strength. Above each plot, the Lewis structures of the two compounds are reported. The atoms of the two rings have been labeled with numbers.

dx.doi.org/10.1021/jp4115018 | J. Phys. Chem. B 2014, 118, 4983−4992

To analyze the spectrum of the 5BU (left panel) let us recall that this molecule is chemically composed of two chromophores: the benzene (model of aromatic amino acid) and the uracil/thymine moieties. Our calculations show that the electronic transitions involve mainly the uracil fragment. This is particularly true for the first two transitions (i.e., those contributing to the absorption spectrum in the lower energetic band). Their character originates from the typical uracil bright $\pi\pi^*$ and dark $n\pi^*$ transitions,[35] while no intrachromophore transitions are observed for the benzene moiety in this energy range. This is because the only transition of benzene accessible in our experimental conditions is the lowest $\pi\pi^*$ electronic transition,[36] which has an oscillator strength much lower than the bright uracil $\pi\pi^*$ transition, and hence, its contribution to the absorption spectrum of 5BU is negligible. The computed uracil transition energies in 5BU are slightly red-shifted compared to the ones relative to pure uracil in similar solutions[23] due to the perturbation induced by the chemical bridging to the second chromophore (benzene). In addition to these intrachromophore transitions, we also observe charge-transfer (CT) excitations from the benzene to the uracil moiety, which contribute to the lower energy band centered at 265 nm in the experimental spectrum (around 60% of the TDDFT absorption line at 248 nm). The corresponding transition densities, defined as the difference between a given electronic excited state density and the density of the ground state,[37] are shown in Figure 3. These functions allow a visualization of the

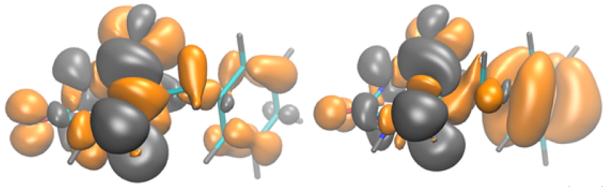

Figure 3. Isosurface plots of the transition densities of the first (left) and second (right) excitations of the 5BU in the Franck–Condon region. Gray indicates positive (electron) and orange negative (hole) contributions.

density changes induced during a particular excitation. In particular, the positive (or negative) part corresponds to the electronic charge accumulation (or hole) created in the ground state electronic density.

To quantify the charge separation induced by the electronic excitation we have integrated the electron/hole density obtained from the positive/negative part of the transition density of the CT excitation. Using TDDFT/M06, we found a partial charge of −0.42 e on uracil and +0.40 e on benzene (the missing 0.02 charge is distributed on the ring substituents).

Interestingly, for the uracil we observe two absorption lines both with mixed $\pi\pi^*$ and $n\pi^*$ character and similar oscillator strengths instead of the two separate bright uracil $\pi\pi^*$ and dark $n\pi^*$ transition observed in gas phase calculations.[36] The origin of the mixing is mainly due to the solvent-induced quasi-degeneracy of the $\pi\pi^*$ and dark $n\pi^*$ transitions. This solvatochromic effect was already detected in studies of solvated uracil performed both via LR-TDDFT methods[23] and wave function based calculations.[38]

Concerning 5,6BU (data shown in the right panel of Figure 2), an unequivocal assignment of the electronic transitions in the range between 250 and 300 nm (that includes the laser wavelength, 260 nm) is not possible because of the weak absorption around 240 nm, which just results in a shallow shoulder in the computed spectrum not resolved experimentally (at room temperature). The first excited state transition is the closest and brightest in that spectral region but, together with this transition, higher energy excitations can be activated.

The cyclization process induces a change in the π-conjugated system of the uracil moiety (disappearance of the enonic group) with consequent loss of the $\pi\pi^*$ transition observed in isolated uracil and 5BU. Characteristics of the 5,6BU are therefore the intrachromophore aromatic $\pi\pi^*$ transition in the benzene moiety (at 240 nm with an oscillator strength of roughly one-third of the $\pi\pi^*$ transition in uracil) and the $n\pi^*$ transition of uracil (see Figure 4, left and right parts,

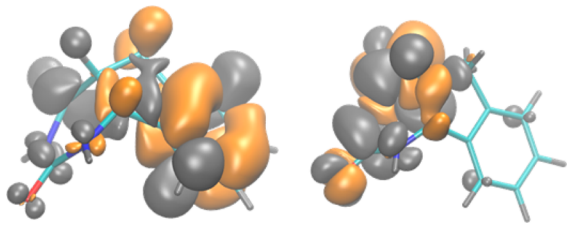

Figure 4. Isosurface plots of the transition densities of the first (left) and second (right) excitations of the 5,6BU in the Franck–Condon region. The color code for the isosurface plots is the same as in Figure 3.

respectively). As for the $\pi\pi^*$ transition in the uracil moiety, the interchromophore CT band observed in 5BU disappears in the photocyclized product. In addition, the second excitation has an almost pure character given by the dark uracil $n\pi^*$ transition (that is no longer mixed with the uracil $\pi\pi^*$ transition, since the latter is missing in 5,6BU) and, accordingly, its oscillator strength becomes zero.

Optical Characterization of the Photocyclization Process. We started the optical characterization of 5BU and 5,6BU by measuring their absorption spectra as a function of the irradiation time. The obtained results are plotted in Figure 5. The change of 5BU into 5,6BU can be considered complete

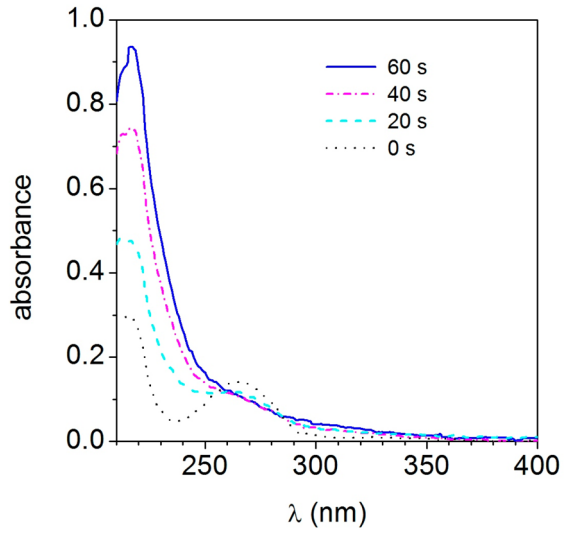

Figure 5. Absorbance of irradiated 5BU. The irradiation time is shown in the legend: dotted, 0 s; dashed, 20 s; dash-dotted, 40 s; and solid line, 60 s. 0 s corresponds to 5BU and 60 s corresponds to 5,6BU.

dx.doi.org/10.1021/jp4115018 | J. Phys. Chem. B 2014, 118, 4983–4992

after 60 s irradiation, since no more significant changes in the spectra are detectable with longer irradiation times. Figure 5 also shows that the 5,6BU absorbance at 220 nm is approximately three times higher than that of 5BU, in agreement with the corresponding oscillator strengths computed with TDDFT. It is worth mentioning that at the laser wavelength (258 nm), both species absorb with a comparable efficiency and that, within experimental errors, an isosbestic point is found at 260 nm. This suggests, already at a pure spectroscopic level, that no photoproduct other than 5,6BU is obtained by UV irradiation.

Similarly to what was done for absorption, fluorescence emission spectra were measured as a function of irradiation time, so that the change of 5BU into 5,6BU could be again followed as a function of the irradiation time. Compared to the absorption, the change in the spectral features is much more striking. Figure 6 shows that a significant shift of the peak from 310 to 360 nm occurs when 5BU is photocyclized into 5,6BU (dotted line t = 0 s versus solid line t = 60 s, in Figure 6).

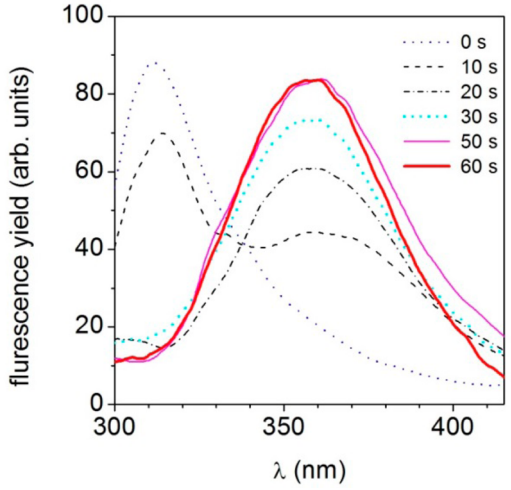

Figure 6. Fluorescence of irradiated 5BU (λ_{exc} = 265 nm). The irradiation time is shown in the legend: dotted, 0 s; dashed, 10 s; dash-dotted, 20 s; short-dashed, 30 s, thin solid line, 50 s; and thick solid line, 60 s. As it will be shown in the following, 0 s corresponds to 5BU and 60 s corresponds to 5,6BU.

Excited States Decay Channels. To interpret these experimental findings, we explored the decay channels of reactant and product also computationally via minimum energy path analysis (geometry relaxations in the electronic excited state). In general, it is known from several quantum chemical calculations[1] that the excited state ultrafast decay of DNA/RNA bases is favored by the existence of barrierless paths that lead to very efficient nonradiative decay processes via conical intersections (CI) with the ground state. Moreover, recent nonadiabatic molecular dynamics studies in gas phase[39] have shown that, after excitation to the $\pi\pi^*$ state, the pyrimidine nucleobases remain mainly trapped into a shallow energy minimum for a time of the order of a few picoseconds before finding their way to a CI with the ground state through a nonradiative path. In our calculations on 5BU, we found a relaxation path on the $\pi\pi^*$ state leading to a stable intermediate state in which a molecular distortion similar to that observed in uracil and thymine occurs. (For the study of this relaxation pathway, the long-range corrected CAM-B3LYP xc functional was used in the calculations. See the Supporting Information for further details).

The molecular structure obtained following this relaxation path is reported in the upper panel of Figure 7 (we refer to this

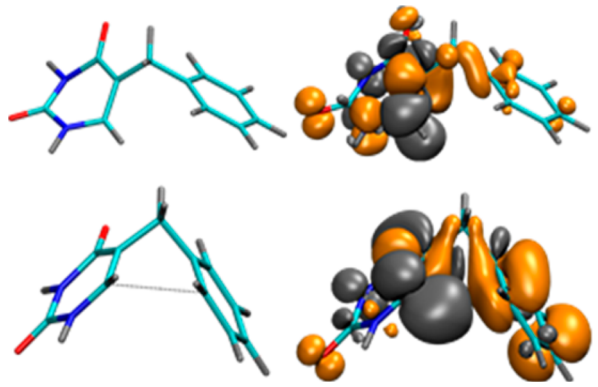

Figure 7. Molecular geometries and corresponding transition densities of 5BU relaxed in the two minima on the $\pi\pi^*$ state. The upper panel is state 1 (see Results and Discussion in the text); the lower panel is state 2. The minimum found with TDDFT/CAM-B3LYP is reported in the upper panel, while the one found with TDDFT/M06 is shown in the lower panel. The color code for the isosurface plots is the same as Figure 3.

as state 1), showing that the structural changes are mainly confined to the uracil moiety (with a heterocyclic ring puckering motion). Similar results have also been reported in gas phase calculations.[36]

In Figure 7, we also show the electronic transition density for this structure, which clearly shows the uracil $\pi\pi^*$ transition dominance in the excited state character. Since experimentally no emission around 330 nm (the computed fluorescence wavelength corresponding to this geometry) is observed, we conclude that this metastable intermediate leads to a nonradiative decay path through CI and is nonemitting, as in the case of thymine and uracil.

We also find that in 5BU, a decay channel not observed in single nucleobases is activated. This relaxation is driven by the CT $\pi\pi^*$ state with a hole on the benzene and excited electron on the uracil moiety, which gives a zwitterionic character to the molecule in the excited state. The relaxed molecular structure on this potential energy surface (PES), state 2, is reported in the bottom panel of Figure 7, where the corresponding transition density is also reported to highlight its CT character. The attraction originating from this charge separation brings the chromophores closer during this relaxation process and brings them toward a stacked configuration. The C5−C6−C15 angle (see Figure 2 for the atom labels) between the two moieties changes from a value of 113° in the Franck−Condon region to a value of 93° in the relaxed CT $\pi\pi^*$ configuration, while the C6−C10 distance decreases from 3.66 to 2.81 Å. We believe that this decay path is responsible for the photoinduced cross-link of 5BU into 5,6BU. In fact, the formation of the C6−C10 covalent bond observed in the cyclized compound might occur thanks to the excess kinetic energy acquired during the excited state relaxation (~2 eV) that could drive the molecular butterfly relaxation motion beyond the (local) minimum of this state (i.e., the molecular structure reported in the lower panel of Figure 7) until the closure of the C6−C10 bond occurs (see Figure S6 in the Supporting Information). Moreover, we have observed that the energy gap between the ground and excited

dx.doi.org/10.1021/jp4115018 | J. Phys. Chem. B 2014, 118, 4983−4992

state at the relaxed structure obtained by constraining the C6−C10 distance to ∼2 Å is small enough to allow a nonadiabatic (nonradiative) surface hop to the ground state (see the Supporting Information for more details).

Finally, the relaxed structures of the sole uracil and 5BU on the nπ* PES are reported in Figure 8, together with the

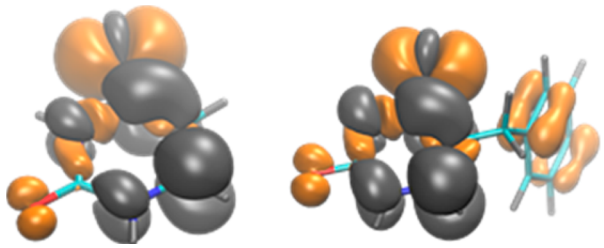

Figure 8. Transition densities for the nπ* state in the relaxed geometry of uracil alone (left) and the 5BU (right). The color code for the isosurface plots is the same as in Figure 3.

isosurface plots of the transition densities. We observe that while the transition in uracil has a pure nπ* character, in 5BU, the nπ* state strongly mixes with the CT ππ* state (see the Supporting Information for more details). The photoemission energy of this configuration is about 311 nm, in good agreement (considering the global blue shift of the TDDFT energies) with the position of the experimental fluorescence peak. Hence, this is the most likely candidate identified by our calculations for the stable radiative state associated to the fluorescence measured experimentally. The mixing of the nπ* state with the CT ππ* state is also probably responsible for the efficiency of the emission, which gains oscillator strength from the ππ* contribution. In Figure 9, we summarize with a cartoon the different deactivation channels of 5BU suggested by our calculations.

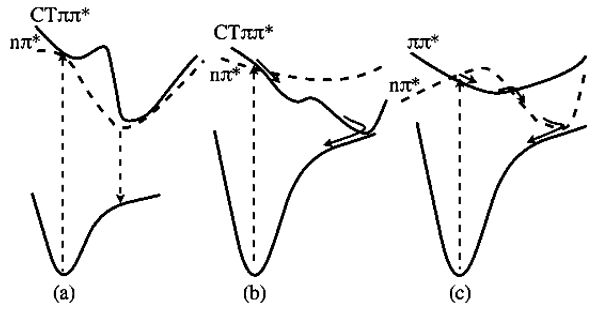

Figure 9. Schematic description of the possible decay paths from the electronic excited states of 5BU based on our calculations: (a) relaxation path via the intrachromophore uracil nπ* state (radiative decay channel); (b) relaxation path via the interchromophore CT ππ* state (nonradiative and reactive decay channel); and (c) relaxation path via the intrachromophore uracil ππ* state (nonradiative and nonreactive decay channel).

In summary, according to our calculations, the photoreactivity of excited 5BU can be attributed to the presence of a CT state characterized by the formation of a (partial) hole on the benzene moiety and the transfer of a fractional charge to the uracil. In this CT state, the two chromophores approach each other because of Coulomb attraction. When they are close, the energy gap between ground and excited states becomes very small and the new covalent bond observed in the cyclized product 5,6BU can eventually be created once the system relaxes back to the electronic ground state (see Figure 9b). Other deactivation channels can be activated involving the uracil moiety, but these intrachromophore transitions are not directly involved in the formation of the cyclized product. In particular, the relaxation on the uracil nπ* state leads to the radiative decay on the ground state (see Figure 9a), while the relaxation on the uracil ππ* state leads to an ultrafast nonradiative decay path similar to those reported in the literature for uracil and thymine[39] (Figure 9c). Note that the relaxation channels described so far do not involve excitations localized solely on the benzene. In fact, while these excitations are clearly possible, they occur at energies higher than those relevant to our experiments: our UV laser irradiates at an energy of 4.8 eV, while the first bright transition in benzene has been found at 6.20 eV.[40]

Finally, it is important to stress that the covalent bond formation between the carbons C6 and C10 in 5BU does not coincide with the generation of the final product 5,6BU. The full reaction mechanism requires an additional tautomerization reaction, causing a proton (or hydrogen) to be transferred from the carbon atom C10 to the carbon atom C5. We believe that, in this step, the solvent plays an important role in the formation of the final cyclized product, possibly via a solvent-assisted proton (or hydrogen) transfer, as hypothesized also by Sun et al.[16] However, to describe this phenomenon, simulations are required in which (at least) part of the solvent is treated explicitly at the DFT/TDDFT level, and in this work we do not address this issue.

We explored computationally also the 5,6BU electronic decay channels to characterize the measured fluorescence. The relaxed photoemission energies and the main relaxed structures with the corresponding transition density isosurfaces are reported in the Supporting Information (Table S4 and Figure S7, respectively). Also in this case, we found a good agreement between the position of the experimental fluorescence peak (350 nm) and the photoemission energy from the energy minimum on the nπ* PES (330 nm). We can therefore conclude that for both 5BU and 5,6BU, the experimentally observed fluorescence in the wavelength range 300−420 nm corresponds to the emission from two different minima on the same nπ* surface (with possible mixing with the CT ππ* state). However, it should be mentioned that in 5,6BU, the decay in the nπ* state is probably not the only fluorescent channel: in fact, as it can be noted from Figure 6, the fluorescence signal remains appreciable (above the baseline) at high energies (∼300 nm) where the emissions from the structures relaxed on the third and sixth excited states are located (for details see Table S5 in the Supporting Information).

Excited States Decay Time. To gain insight into the electronic relaxation timescale of the 5BU and 5,6BU, we also measured the fluorescence anisotropy through the polarization coefficient[41] $A = (I_{\parallel} - I_{\perp})/(I_{\parallel} + I_{\perp})$ as a function of the laser irradiation time. In the definition of the polarization coefficient, $I_{\parallel}$ and $I_{\perp}$ are the fluorescence yield polarized parallel and orthogonal to the polarization direction of the incident beam, respectively. The results are reported in Figure 10 and show that $A \approx 0.5$ at $t = 0$ [i.e., when only 5BU is in the solution] and reduces to approximately 0.17 for long irradiation time when 5BU is completely photocyclized (i.e., for 5,6BU).

It is known that the timescale of the rotational relaxation time of organic dyes having shape and steric hindrance similar to 5BU and 5,6BU in MeOH solution lies in the subnano-

dx.doi.org/10.1021/jp4115018 | J. Phys. Chem. B 2014, 118, 4983−4992

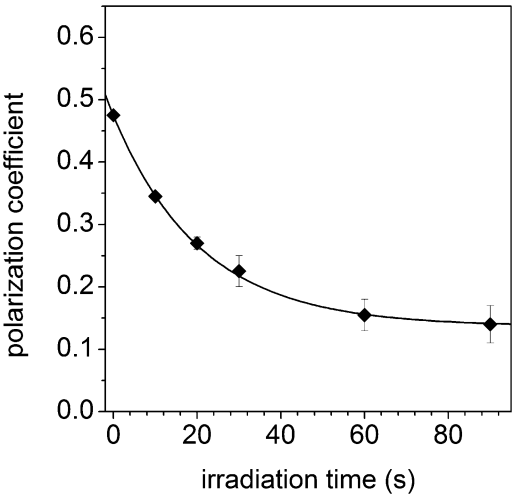

Figure 10. Anisotropy of the fluorescence emission as a function of the irradiation time measured at λ = 320 nm. At t = 0 s, only 5BU is present which photocyclizes to 5,6BU when irradiated. The continuous line is the best fit with the function $f(t) = a + b \exp(-t/\tau)$ (see main text) that leads to τ = 20.9 ± 0.6 s. The error bars come from the uncertainty in the measurement of the fluorescence yield propagated in the equation for the polarization coefficient.

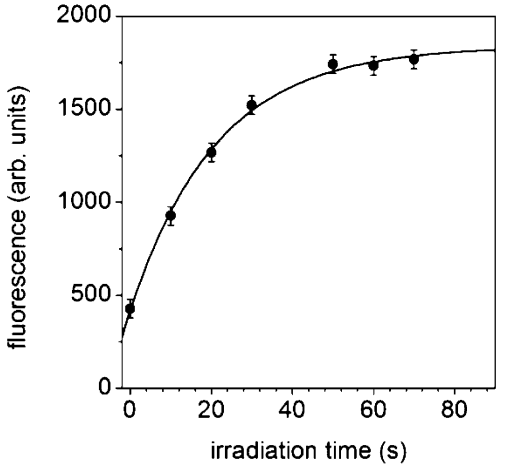

Figure 11. Fluorescence yield of the irradiated solution in the range of 355−365 nm as a function of the irradiation time. The continuous line is the best fit with the function $f(t) = a + b \exp(-t/\tau)$ that leads to τ = 21.3 ± 1.4 s.

second range (70−80 ps).[42,43] Therefore, the same timescale can be reasonably assumed for the rotational relaxation time of 5BU and 5,6BU. As a consequence, the high value of anisotropy found for 5BU implies that its fluorescence signal has to decay in a timescale of a few picoseconds. This confirms that the proximity of the benzene moiety to the uracil in 5BU does not perturb significantly the electronic structure of the uracil side and the molecule preserves its ultrafast decay properties. This experimental observation is somewhat surprising since it sets 5BU apart from other compounds obtained via chemical substitution on the uracil carbon C5. In fact, experiments in which the effects of other substituents (e.g., 5-OH-Ura and 5-NH2-Ura) were studied, consistently showed that the excited state lifetime significantly increases upon substitution (to nanosecond or more).[44] On the other hand, the lower anisotropy in the 5,6BU is a signature of a decay time lying in the range of nanoseconds. This can be ascribed to the changes in the electronic structure which, as discussed above, entail the disappearance of the uracil $\pi\pi^*$ transition in 5,6BU of the π−π^* uracil excited PES, which is responsible for the ultrafast decay time of 5BU.

Photocyclization QY. The features observed in the fluorescence spectra reported in Figure 6 allow an indirect measurement of the photocyclization QY (p_{pc} in the following), via the knowledge of the characteristic time for 5BU → 5,6BU transformation. To show this, we report the fluorescence yield in the 355−365 nm range as a function of the irradiation time in Figure 11. This plot shows that the collected fluorescence signal saturates after approximately 1 min of irradiation at 0.2 W. This behavior can be explained by considering the occurrence of the reaction $h\upsilon$ + 5BU → 6BU together with the conservation of the number of molecules; hence we have

$$\frac{d}{dt}N_{pc}(t) = \frac{N_{5BU}(t)}{\tau}$$
$$N_{5BU}(t) + N_{pc}(t) = N_{5BU}(0) \quad (1)$$

where t is the irradiation time and N_{5BU} and N_{pc} are the concentration of 5BU and 5,6BU, respectively. In eq 1, τ is the characteristic time for the transformation of 5BU into 5,6BU and is given by

$$\tau = \frac{1}{f_L p_{abs} p_{pc}} \quad (2)$$

where f_L is the repetition rate of the laser (2 kHz), p_{abs} is the probability that a molecule absorbs one photon in a single laser pulse, and p_{pc} is the probability that the excited molecule will photocyclize (i.e., p_{pc} is the photocyclization quantum yield).

The assumption of $\tau \gg \tau_{eq}$, τ_{eq} being the time required for homogenizing the solution, is necessary for the validity of eq 1 and is well-fulfilled in our conditions (i.e., we can reasonably assume that the gradient in the 5,6BU concentration between irradiated and not irradiated volume is negligible).

Since the fluorescence signal is proportional to the concentration and the latter can be easily derived from eq 1, we have the following relation for the overall fluorescence detected in the wavelength range of 355−365 nm:

$$\mathrm{FY}(t) = k_{inst} N_{5BU}(0)\left[FY_{pc} - (FY_{pc} - FY_{5BU}) \exp\left(-\frac{t}{\tau}\right)\right] \quad (3)$$

In eq 3, FY_{pc} and FY_{5BU} are the fluorescence quantum yields of 5,6BU and 5BU, respectively, and k_{inst} is an instrumental constant. The best fit of the experimental data in Figure 11 with a function like that in eq 3 allows us to estimate the characteristic photocyclization time as τ = 21.3 ± 1.4 s.

To check the validity of this estimate, we considered also the dependence of the polarization coefficient A on the irradiation time (see Figure 10) that follows a law similar to eq 3. For instance, we have

$$A(t) = A_{pc} - (A_{pc} - A_{5BU}) \exp\left(-\frac{t}{\tau}\right) \quad (4)$$

where A_{5BU} and A_{pc} are the polarization coefficients of the 5BU and 5,6BU, respectively. The best fit of the experimental results in Figure 10 allows us to estimate the characteristic photocyclization time as τ = 20.9 ± 0.6 s in very good agreement with

dx.doi.org/10.1021/jp4115018 | J. Phys. Chem. B 2014, 118, 4983−4992

the estimation through fluorescence yield. From the two independent measurements we have the combined estimation of this time as $\tau = 21.0 \pm 0.6$ s.

Apart from p_{pc}, the only remaining unknown quantity in eq 2 is p_{abs}, which can be estimated as follows. Far from the saturation (linear absorption) the probability that a photon is absorbed by a molecule is proportional to the photon number (N_f) and to the absorption cross section σ_{abs}, thus,

$$p_{abs} = \frac{N_f \sigma_{abs}}{S} = \frac{E_{pulse}\sigma_{abs}}{h\nu S} \quad (5)$$

where S is the effective area illuminated by the laser. In our conditions, this area coincides with the section of the cuvette, since the mixing is fast enough to consider the solution homogeneous. We have measured the absorptivity (ε) of the 5BU to be 11900 mol^{-1} cm^{-1}, which in turn provides σ_{abs} (cm^2) = $3.82 \times 10^{-21}\varepsilon$ (mol^{-1} cm^{-1}) = 4.5×10^{-17}. Since we have $E_{pulse} = 170$ μJ, $h\nu = 4.8$ eV ($\lambda = 258$ nm), and $S = 1$ cm^2, the probability that in our experimental condition a photon is absorbed by a 5BU molecule is $p_{abs} = 10^{-2}$. From eq 1, by considering $f = 2$ kHz, we have $p_{pc} = 2.4 \times 10^{-3}$ in excellent agreement with Sun et al.[16]

Fluorescence QY Measurement. The fluorescence QY of 5BU and 5,6BU is provided by[45]

$$QY_X = QI_R \frac{I_X OD_R n_X^2}{I_R OD_X n_R^2} \quad (6)$$

where OD stands for the optical density (absorbance), I for the fluorescence intensity, and n for the refraction index, the subscripts X and R referring to the molecule whose QY has to be measured and to the reference, respectively. Since 5BU is diluted in methanol and the reference molecule (tryptophan) in water, we have $n_X \approx n_R$, and hence,

$$QY_X = QI_{try} \frac{slope_X}{slope_{try}} \quad (7)$$

In eq 7, slope refers to the slopes in Figure 12 and X stands for 5BU or 5,6BU, respectively. By using $QY_{try} = 0.13 \pm 0.01$ as reported in literature,[45] we have $QY_{5BU} = 0.11 \pm 0.02$ and $QY_{5,6BU} = 0.38 \pm 0.02$. These values represent the first measurements of the fluorescence quantum yields for 5BU and 5,6BU. QY for both molecules are 4 orders of magnitude higher than fluorescence QY for thymine and uracil.[46]

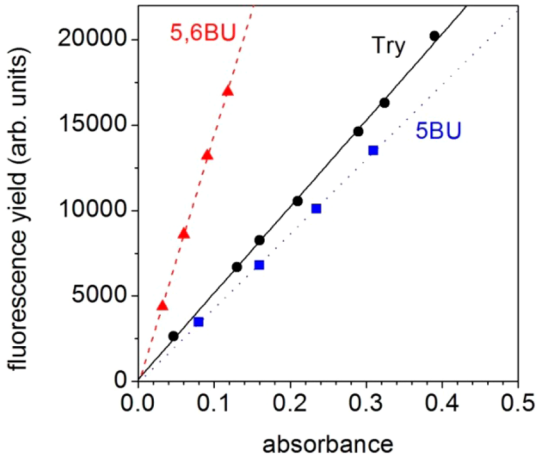

Figure 12. Fluorescence vs absorbance for 5BU, 5,6BU, and tryptophan ($\lambda_{exc} = 278$ nm), the latter used as standard.

The relatively high fluorescence QY in 5BU can be explained with the lack of some of the nonradiative decay channels which are active in the DNA and RNA bases. Indeed, for these molecules and in particular for isolated uracil and thymine, nonadiabatic dynamics studies in the gas phase[39] show that after photoexcitation into the bright $\pi\pi^*$ state, the molecules can decay via two main nonradiative pathways. Following the first pathway, the molecule relaxes into the lower-lying $n\pi^*$ state and from there into the ground state via a CI. The other relaxation pathway leads to the ground state directly from the $\pi\pi^*$ state via a CI. The second (faster) relaxation channel has a different relevance for the two bases being more effective for uracil than for thymine (such a difference can also explain the shorter lifetime of the uracil excitation which has been observed experimentally).[47] This is probably due to the need of an out-of-plane motion of the 5-substituent for its activation.[35] Uracil has an H atom in this position, while thymine has a methyl group. The steric hindrance of the methyl, which limits the out-of-plane motion, frustrates the role played by the second relaxation channel for thymine compared to its importance in uracil. This argument suggests that for 5BU, the second relaxation channel, if not completely suppressed, is even more inhibited than for thymine. In fact, in 5BU, the 5-substituent is an entire phenyl group whose steric hindrance is larger than that of the methyl. This hypothesis is also supported by the calculations performed by Micciarelli et al.[36] on 5BU, where no CI has been found directly connecting the $\pi\pi^*$ PES to the ground state. Thus, the suppression of this decay channel favors the radiative decay, explaining the high fluorescence QY. Following this argument, the even higher fluorescence QY in 5,6BU and its longer fluorescence lifetime result from the lack of the uracil $\pi\pi^*$ transition and, hence, also of the ultrafast $\pi\pi^* \rightarrow n\pi^{**} \rightarrow$ ground state nonradiative decay channel.

CONCLUSIONS

In conclusion, we reported and discussed the main photophysical and photochemical properties of 5BU and 5,6BU by using a combined experimental (spectroscopy) and theoretical (electronic structure calculations) approach. We showed that irradiation of 5BU with high intensity UV femtosecond pulses (Figure 1, left panel) in MeOH solution leads to the formation of a cyclized compound: 5,6BU (Figure 1, right panel). This photoreaction mimics the formation of a cross-link between a pyrimidine nucleobase and a close-lying aromatic amino acid.

The spectroscopic data allowed us to measure the value of 2.4×10^{-3} for the photocyclization QY in excellent agreement with the previous measurements of Sun et al.[16] The fluorescence QY and fluorescence anisotropy of 5BU and 5,6BU have also been measured for the first time. Interestingly, the fluorescence QYs of both molecules are found to be very high (i.e., four orders of magnitude larger than the QY of single nucleobases in solution). Moreover, the fluorescence anisotropy measurements revealed that the fluorescence signal of the 5BU decays in the ultrafast timescale of few picoseconds, a property which is lost when the molecule takes the cyclized form for 5,6BU.

The observed ultrafast decay properties of 5BU can be ascribed to the fact that the main excited state properties of the nucleobases remain almost unchanged in 5BU (we detected the presence of a decay path similar to the one responsible for nonradiative decay to the ground state in isolated uracil/

dx.doi.org/10.1021/jp4115018 | J. Phys. Chem. B 2014, 118, 4983−4992

thymine). However, the same cannot be said for the different decay channel branching ratios: as proved by the high fluorescence QY; in fact, the radiative decay channel (that we identified in the relaxation of the molecule on the uracil nπ^* state) is more favored in 5BU than in the DNA bases alone. This behavior can be explained with the inhibition of the out-of-plane motion of the 5-substituent due to the presence of the phenyl group. This hinders the nonradiative relaxation pathway that in uracil and thymine leads to the ground state directly from the bright $\pi\pi^*$ state via a CI.

The higher decay time of 5,6BU has instead to be ascribed to the changes in the electronic structure induced by the loss of the electronic π-conjugation associated with the enone chemical group of the DNA bases. As a consequence, the bright uracil $\pi\pi^*$ transition is no longer observed in 5,6BU, causing the disappearance of all the ultrafast decay channels associated with this transition.

The global picture emerging from the combination of the theoretical and computational results leads to the conclusion that the use of 5BU as a model system to study the proximity relations of a DNA base with a close-lying aromatic amino acid is valid at a local level: we observe that the main characteristics of the decay processes from the excited states of the uracil/thymine molecules remain almost unchanged in 5BU and the main perturbation observed is caused by the presence of the close-lying aromatic group. In particular, this moiety entails the formation of a CT electronic transition, leading to photoreactivity after the absorption of one photon. Of course, since in this model system only two chromophores are present, alternative mechanisms involving more than two partners in a biological environment cannot be discarded or captured. In particular, in a more extended system, multiphoton absorption processes may play a role.

Finally, the high fluorescence QY of both molecules, together with strong differences in their absorption spectra and fluorescence spectra, lifetime, and anisotropy, call for spectroscopic time-resolved experiments that, together with nonadiabatic excited states molecular dynamics simulations, will allow a more detailed study of the photoreaction mechanism. Future computational work, in which 5BU and the solvent are treated explicitly within a QM/MM representation, will also focus on investigating the role of the solvent in the tautomerization event which (most likely) completes the formation of 5,6BU after the formation of the C6−C10 covalent bond discussed in this work.

■ ASSOCIATED CONTENT

Supporting Information

The quality of the DFT/TDDFT exchange-correlation functionals is assessed by means of benchmark calculations. We also report additional details about the description of the decay channels observed for 5BU and 5,6BU using LR-TDDFT calculations. This material is available free of charge via the Internet at http://pubs.acs.org.

■ AUTHOR INFORMATION

Corresponding Authors

*E-mail: ivano.tavernelli@epfl.ch.
*E-mail: rvelotta@unina.it.

Notes

The authors declare no competing financial interest.

■ ACKNOWLEDGMENTS

M.M., B.D.V., and S.B. acknowledge financial support from the Italian Institute of Technology (Grant IIT-SEED Project N 259 SIMBEDD).

■ REFERENCES

(1) Markovitsi, D.; Gustavsson, T.; Banyasz, A. Absorption of UV Radiation by DNA: Spatial and Temporal Features. *Mutat. Res.* **2010**, *704*, 21−28.
(2) Gustavsson, T.; Banyasz, A.; Improta, R.; Markovitsi, D. Femtosecond Fluorescence Studies of DNA/RNA Constituents. *J. Phys.: Conf. Ser.* **2011**, *261*, 012009.
(3) Canuel, C.; Mons, M.; Piuzzi, F.; Tardivel, B.; Dimicoli, I.; Elhanine, M. Excited States Dynamics of DNA and RNA Bases: Characterization of a Stepwise Deactivation Pathway in the Gas Phase. *J. Chem. Phys.* **2005**, *122*, 074316.
(4) Blancafort, L.; Cohen, B.; Hare, P. M.; Kohler, B.; Robb, M. Singlet Excited-State Dynamics of 5-Fluorocytosine and Cytosine: An Experimental and Computational Study. *J. Phys. Chem. A* **2005**, *109*, 4431−4436.
(5) Görner, H. New Trends in Photobiology. *J. Photochem. Photobiol., B* **1994**, *26*, 117−139.
(6) Masson, F.; Laino, T.; Tavernelli, I.; Rothlisberger, U.; Hutter, J. Computational Study of Thymine Dimer Radical Anion Splitting in the Self-Repair Process of Duplex DNA. *J. Am. Chem. Soc.* **2008**, *130*, 3443−3450.
(7) Masson, F.; Laino, T.; Rothlisberger, U.; Hutter, J. A QM/MM Investigation of Thymine Dimer Radical Anion Splitting Catalyzed by DNA Photolyase. *ChemPhysChem* **2009**, *10*, 400−410.
(8) Giussani, A.; Serrano-Andrés, L.; Merchán, M.; Roca-Sanjuán, D.; Garavelli, M. Photoinduced Formation Mechanism of the Thymine-Thymine (6−4) Adduct. *J. Phys. Chem. B* **2013**, *117*, 1999−2004.
(9) Cuquerella, M. C.; Lhiaubet-Vallet, V.; Bosca, F.; Miranda, M. A. Photosensitised Pyrimidine Dimerisation in DNA. *Chem. Sci.* **2011**, *2*, 1219.
(10) Schreier, W. J.; Schrader, T. E.; Koller, F. O.; Gilch, P.; Crespo-Hernández, C. E.; Swaminathan, V. N.; Carell, T.; Zinth, W.; Kohler, B. Thymine Dimerization in DNA Is an Ultrafast Photoreaction. *Science* **2007**, *315*, 625−629.
(11) Moss, T.; Dimitrov, S. I.; Houde, D. UV-Laser Crosslinking of Proteins to DNA. *Methods: A Companion to Methods in Enzymology* **1997**, *11*, 225−234.
(12) Lejnine, S.; Durfee, G.; Murnane, M.; Kapteyn, H. C.; Makarov, V. L.; Langmore, J. P. Crosslinking of Proteins to DNA in Human Nuclei Using a 60 fs 266 Nm Laser. *Nucleic Acids Res.* **1999**, *27*, 3676−3684.
(13) Barker, S.; Weinfeld, M.; Murray, D. DNA-Protein Crosslinks: Their Induction, Repair, and Biological Consequences. *Mutat. Res.* **2005**, *589*, 111−135.
(14) Altucci, C.; Nebbioso, a.; Benedetti, R.; Esposito, R.; Carafa, V.; Conte, M.; Micciarelli, M.; Altucci, L.; Velotta, R. Nonlinear Protein-Nucleic Acid Crosslinking Induced by Femtosecond UV Laser Pulses in Living Cells. *Laser Phys. Lett.* **2012**, *9*, 234−239.
(15) Zhang, L.; Zhang, K.; Prändl, R.; Schöffl, F. Detecting DNA-Binding of Proteins in Vivo by UV-Crosslinking and Immunoprecipitation. *Biochem. Biophys. Res. Commun.* **2004**, *322*, 705−711.
(16) Sun, G.; Fecko, C. J.; Nicewonger, R. B.; Webb, W. W.; Begley, T. P. DNA-Protein Cross-Linking: Model Systems for Pyrimidine-Aromatic Amino Acid Cross-Linking. *Org. Lett.* **2006**, *8*, 681−683.
(17) Jean-Ruel, H.; Cooney, R. R.; Gao, M.; Lu, C.; Kochman, M. A.; Morrison, C. A.; Miller, R. J. D. Femtosecond Dynamics of the Ring Closing Process of Diarylethene: A Case Study of Electrocyclic Reactions in Photochromic Single Crystals. *J. Phys. Chem. A* **2011**, *115*, 13158−13168.
(18) Aldoshin, S. M.; Yuŕeva, E. A.; Sanina, N. A.; Krayushkin, M. M.; Tsyganov, D. V.; Gostev, F. E.; Shelaev, I. V.; Sarkisov, O. M.; Nadtochenkoa, V. A. Femtosecond Dynamics of Photocyclization of 1-[(4-{5-[4-Chloromethyl-2,5-Dimethyl-3-Thienyl]-2-Oxo-1,3-Dioxol-4-

Yl}- 2,5-Dimethyl-3-Thienyl)methyl]pyridinium Chloride. *Russian Chemical Bulletin, International Edition* **2011**, *60*, 1118−1127.
(19) Siewertsen, R.; Renth, F.; Temps, F.; Sönnichsen, F. Parallel Ultrafast E-C Ring Closure and E-Z Isomerisation in a Photochromic Furylfulgide Studied by Femtosecond Time-Resolved Spectroscopy. *Phys. Chem. Chem. Phys.* **2009**, *11*, 5952−5961.
(20) Natali, M.; Giordani, S. Molecular Switches as Photocontrollable "Smart" Receptors. *Chem. Soc. Rev.* **2012**, *41*, 4010−4029.
(21) Leang, S. S.; Zahariev, F.; Gordon, M. S. Benchmarking the Performance of Time-Dependent Density Functional Methods. *J. Chem. Phys.* **2012**, *136*, 104101.
(22) Goerigk, L.; Grimme, S. A Thorough Benchmark of Density Functional Methods for General Main Group Thermochemistry, Kinetics, and Noncovalent Interactions. *Phys. Chem. Chem. Phys.* **2011**, *13*, 6670−6688.
(23) Improta, R.; Barone, V. Absorption and Fluorescence Spectra of Uracil in the Gas Phase and in Aqueous Solution: A TD-DFT Quantum Mechanical Study. *J. Am. Chem. Soc.* **2004**, *126*, 14320−14321.
(24) Dreuw, A.; Head-Gordon, M. Failure of Time-Dependent Density Functional Theory for Long-Range Charge-Transfer Excited States: The Zincbacteriochlorin-Bacteriochlorin and Bacteriochlorophyll-Spheroidene Complexes. *J. Am. Chem. Soc.* **2004**, *126*, 4007−4016.
(25) Li, R.; Zheng, J.; Truhlar, D. G. Density Functional Approximations for Charge Transfer Excitations with Intermediate Spatial Overlap. *Phys. Chem. Chem. Phys.* **2010**, *12*, 12697−12701.
(26) Eriksen, J. J.; Sauer, S. P. a.; Mikkelsen, K. V.; Christiansen, O.; Jensen, H. J. A.; Kongsted, J. Failures of TDDFT in Describing the Lowest Intramolecular Charge-Transfer Excitation in Para -Nitroaniline. *Mol. Phys.* **2013**, *111*, 1235−1248.
(27) Frisch, M. J.; Trucks, G. W.; Schlegel, H. B.; Scuseria, G. E.; et al. *Gaussian 09*, revision A.1; Gaussian Inc.: Wallingford, CT, 2009.
(28) Perdew, J.; Burke, K.; Ernzerhof, M. Generalized Gradient Approximation Made Simple. *Phys. Rev. Lett.* **1996**, *77*, 3865−3868.
(29) Zhao, Y.; Truhlar, D. G. The M06 Suite of Density Functionals for Main Group Thermochemistry, Thermochemical Kinetics, Noncovalent Interactions, Excited States, and Transition Elements: Two New Functionals and Systematic Testing of Four M06-Class Functionals and 12 Other Function. *Theor. Chem. Acc.* **2007**, *120*, 215−241.
(30) Yanai, T.; Tew, D. P.; Handy, N. C. A New Hybrid Exchange−Correlation Functional Using the Coulomb-Attenuating Method (CAM-B3LYP). *Chem. Phys. Lett.* **2004**, *393*, 51−57.
(31) Kendall, R. A.; Dunning, T. H.; Harrison, R. J. Electron Affinities of the First-Row Atoms Revisited. Systematic Basis Sets and Wave Functions. *J. Chem. Phys.* **1992**, *96*, 6796.
(32) Scalmani, G.; Frisch, M. J.; Mennucci, B.; Tomasi, J.; Cammi, R.; Barone, V. Geometries and Properties of Excited States in the Gas Phase and in Solution: Theory and Application of a Time-Dependent Density Functional Theory Polarizable Continuum Model. *J. Chem. Phys.* **2006**, *124*, 94107.
(33) The Official Gaussian Website. http://www.gaussian.com/ (accessed September 11, 2013).
(34) Peach, M. J. G.; Benfield, P.; Helgaker, T.; Tozer, D. J. Excitation Energies in Density Functional Theory: An Evaluation and a Diagnostic Test. *J. Chem. Phys.* **2008**, *128*, 044118.
(35) Kistler, K. A.; Matsika, S. Three-State Conical Intersections in Cytosine and Pyrimidinone Bases. *J. Chem. Phys.* **2008**, *128*, 215102.
(36) Micciarelli, M.; Altucci, C.; Della Ventura, B.; Velotta, R.; Toşa, V.; Pérez, A. B. G.; Rodríguez, M. P.; de Lera, A. R.; Bende, A. Low-Lying Excited-States of 5-Benzyluracil. *Phys. Chem. Chem. Phys.* **2013**, *15*, 7161−7173.
(37) Ullrich, C. A. *Time-Dependent Density-Functional Theory. Concepts and Appli- Cations*; Oxford University Press Inc.: New York, 2012; pp 145−148.
(38) DeFusco, A.; Ivanic, J.; Schmidt, M. W.; Gordon, M. S. Solvent-Induced Shifts in Electronic Spectra of Uracil. *J. Phys. Chem. A* **2011**, *115*, 4574−4582.
(39) Barbatti, M.; Aquino, A. J. a; Szymczak, J. J.; Nachtigallová, D.; Hobza, P.; Lischka, H. Relaxation Mechanisms of UV-Photoexcited DNA and RNA Nucleobases. *Proc. Natl. Acad. Sci. U.S.A.* **2010**, *107*, 21453−21458.
(40) Thompson, A. L.; Martínez, T. J. Time-Resolved Photoelectron Spectroscopy from First Principles: Excited State Dynamics of Benzene. *Faraday Discuss.* **2011**, *150*, 293−311.
(41) Valeur, B. *Molecular Fluorescence: Principles and Applications*; Wiley-VCH Verlag GmbH: Weinheim, 2001; pp 353−355.
(42) Zhou, P.; Song, P.; Liu, J.; Han, K.; He, G. Experimental and Theoretical Study of the Rotational Reorientation Dynamics of 7-Aminocoumarin Derivatives in Polar Solvents: Hydrogen-Bonding Effects. *Phys. Chem. Chem. Phys.* **2009**, *11*, 9440−9449.
(43) Kurnikova, M. G.; Balabai, N.; Waldeck, D. H.; Coalson, R. D. *Rotational Relaxation in Polar Solvents. Molecular Dynamics Study of Solute-Solvent Interaction* **1998**, *7863*, 6121−6130.
(44) Nachtigallová, D.; Lischka, H.; Szymczak, J. J.; Barbatti, M.; Hobza, P.; Gengeliczki, Z.; Pino, G.; Callahan, M. P.; de Vries, M. S. The Effect of C5 Substitution on the Photochemistry of Uracil. *Phys. Chem. Chem. Phys.* **2010**, *12*, 4924−4933.
(45) Lakowicz, J. R. *Principles of Fluorescence Spectroscopy*, 3rd ed.; Springer: New York, 2006.
(46) Daniels, M.; Hauswirth, W. Fluorescence of the Purine and Pyrimidine Bases of the Nucleic Acids in Neutral Aqueous Solution at 300 K. *Science* **1971**, *171*, 675−677.
(47) Gustavsson, T.; Bányász, A.; Lazzarotto, E.; Markovitsi, D.; Scalmani, G.; Frisch, M. J.; Barone, V.; Improta, R. Singlet Excited-State Behavior of Uracil and Thymine in Aqueous Solution: A Combined Experimental and Computational Study of 11 Uracil Derivatives. *J. Am. Chem. Soc.* **2006**, *128*, 607−619.